Princeton Plasma Physics Laboratory

PPPL-5254

Equilibrium Potential Well due to Finite Larmor Radius Effects at the Tokamak Edge

W.W. Lee, R. B. White

August 2016

Prepared for the U.S.Department of Energy under Contract DE-AC02-09CH11466.

Princeton Plasma Physics Laboratory
Report Disclaimers

Full Legal Disclaimer

This report was prepared as an account of work sponsored by an agency of the United States Government. Neither the United States Government nor any agency thereof, nor any of their employees, nor any of their contractors, subcontractors or their employees, makes any warranty, express or implied, or assumes any legal liability or responsibility for the accuracy, completeness, or any third party's use or the results of such use of any information, apparatus, product, or process disclosed, or represents that its use would not infringe privately owned rights. Reference herein to any specific commercial product, process, or service by trade name, trademark, manufacturer, or otherwise, does not necessarily constitute or imply its endorsement, recommendation, or favoring by the United States Government or any agency thereof or its contractors or subcontractors. The views and opinions of authors expressed herein do not necessarily state or reflect those of the United States Government or any agency thereof.

Trademark Disclaimer

Reference herein to any specific commercial product, process, or service by trade name, trademark, manufacturer, or otherwise, does not necessarily constitute or imply its endorsement, recommendation, or favoring by the United States Government or any agency thereof or its contractors or subcontractors.

PPPL Report Availability

Princeton Plasma Physics Laboratory:

http://www.pppl.gov/techreports.cfm

Office of Scientific and Technical Information (OSTI):

http://www.osti.gov/scitech/

Related Links:

U.S. Department of Energy

U.S. Department of Energy Office of Science

U.S. Department of Energy Office of Fusion Energy Sciences

Equilibrium Potential Well due to Finite Larmor Radius Effects at the Tokamak Edge

W. W. Lee[1,*] and R. B. White[1]

[1]*Plasma Physics Laboratory, Princeton University, P.O.Box 451, Princeton, New Jersey 08543*

Abstract

We present a novel mechanism for producing the equilibrium potential well near the edge of a tokamak. Briefly, because of the difference in gyroradii between electrons and ions, an equilibrium electrostatic potential is generated in the presence of spatial inhomogeneity of the background plasma, which, in turn, produces a well associated with the radial electric field, E_r, as observed at the edge of many tokamak experiments. We will show that this theoretically predicted E_r field, which can be regarded as producing a long radial wave length zonal flow, agrees well with recent experimental measurements. The relationship between the equilibrium configuration used in the present study and that of the Woltjer-Taylor state will be discussed.

PACS numbers: 52.20.Dq, 52.30.Gz

*Electronic address: `wwlee@pppl.gov`

Let us start by first defining the meaning of "quasineutrality" ($n_i \approx n_e$) associated with study of microturbulence and zonal flows, where "absolute neutrality" is not of interest. Due to finite Larmor radius (FLR) effects of the ions, from the gyrokinetic point of view [1], the ion number density is made up of three parts. Charge densities become $n_i = n_i^{gc} + n_i^{pol} + n_i^{inho}$ and $n_e = n_e^{gc}$, the ion gyrocenter density, n_i^{gc}, the ion polarization density, n_i^{pol}, and the ion gyrocenter density associated with the background inhomogeneity, n_i^{inho}. On the other hand, the electron number density is assumed to be the same as the electron guiding center density. As such, the quasineutral condition now becomes

$$n_i^{gc} + n_i^{pol} + n_i^{inho} = n_e^{gc}, \tag{1}$$

where n_i^{pol} is associated with the electrostatic potential ϕ [1], replacing the usual Coulomb potential term in Poisson's equation. Most gyrokinetic calculations based on Eq. 1 have not taken into account the n_i^{inho} term, since it is always deemed small. If $n_i^{gc} = n_e^{gc}$, we then have $n_i^{pol} = 0$, i.e., $\phi \approx 0$ and we are, therefore, in equilibrium. However, n_i^{inho} can become significant due to the difference between the ion gyrocenter density and the electron guiding center density in the vicinity of strong density and or temperature gradients, for example near the transport pedestal in H-mode discharges. To verify the validity of Eq. 1 for such a scenario, we have carried out a simulation using a cylindrical code by following the full cyclotron motion of the ions (instead of gyrokinetic ions) in a distribution with a strong density gradient. By recording the particle positions as well as the guiding center positions at each time step, we then proceed to calculate the resulting potentials and other associated quantities. For the initial condition for the simulation of $n_i^{gc} = n_e^{gc}$, we look for a possible equilibrium solution associated with

$$n_i^{pol} + n_i^{inho} = 0. \tag{2}$$

Note that we are not looking for *"the"* equilibrium solution with absolute neutrality. On the other hand, we can justify our present model based on the fluid point of view for the two species involved.

Introduce with Monte Carlo methods a particle density of

$$\frac{n(r)}{n_0} = \frac{1}{2} - \frac{tanh[(r - r_0)/w]}{2} + n_s, \tag{3}$$

where n_s is the value outside the pedestal, with the relationship between the gyrocenter

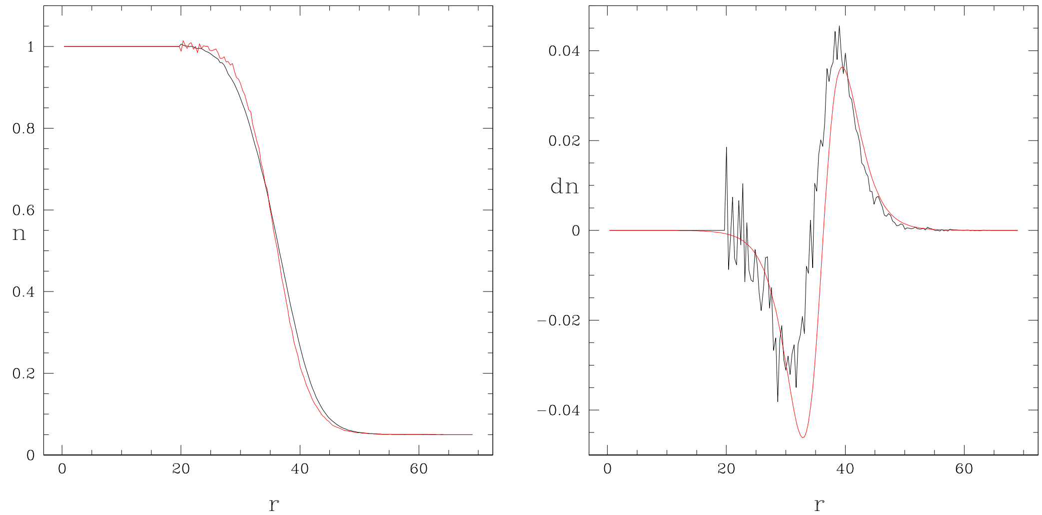

FIG. 1: Plots of particle and gyro center densities as a function of minor radius, in cm, with particle density in black and gyro center density in red at left, and at the right the difference, shown in black, with the analytic expression Eq. 5 shown in red. Gyro radius $\rho_i = 2.3$ cm, $w = 5$ cm, and $r_0 = 36$ cm.

position ($\mathbf{R}$) and the particle position ($\mathbf{x}$) for each particle given by

$$\mathbf{R} = \mathbf{x} + \frac{\mathbf{v} \times \mathbf{B}}{\alpha B^2}, \tag{4}$$

where in Eq. 3 r is the radial component of the position, $\alpha \equiv q/mc$, and q and m are the charge and mass for the particles involved. The difference in the particle and gyrocenter densities is given analytically by the expression[1, 3]

$$n = n_{gc} + \delta n = n_{gc} + \frac{1}{2T_i}\rho_i^2 \nabla_\perp^2 n_{gc} T_i = n_{gc} + \frac{\rho_i^2}{2T_i}\left(\frac{\partial^2 n_{gc} T_i}{\partial^2 r} + \frac{1}{r}\frac{\partial n_{gc} T}{\partial r}\right), \tag{5}$$

for a simulation system which is much larger than the ion Larmor radius ρ_i. Here T_i is the ion temperature. If we assume that the electron distribution is the same as the ion gyro center distribution this leads to an extra charge distribution. This assumption leads to a distribution which is not quasi neutral, but we explore its consequences and its relationship to the Woltjer-Taylor state of $\nabla \times \mathbf{B} = \alpha \mathbf{B}$, where α is a constant.

As a model test case we take a circular equilibrium with major radius $R = 164$, minor radius $a = 69$, and a density distribution given by Eq. 3, with $r_0 = 36$, $w = 5$, all in cm. The particle distribution was taken to be monoenergetic, with particle energy of 50 keV and $B_0 = 20kG$, giving $\rho_i = 2.3cm$. Particles are stepped following full gyro motion in cylindrical geometry using a fourth order Runge Kutta algorithm[2]. After loading, 2×10^6 particles were stepped for 500 cyclotron periods, with data on densities recorded every time step in 200 bins in minor radius, giving maximum density of 4×10^8 particles per bin. Computing took 15 hours of CPU. Plotted in Fig. 1 are analytic and numerical simulation values. Within statistical error we see reasonable agreement with the theoretical prediction. To obtain these results it is essential that the gradient scale length, the particle gyro radius, and the numerical bins for measuring the distribution be of the same order. For this reason it is better to use a monoenergetic distribution.

From Eq. (5), the extra ion charge density gives rise to an electrostatic potential via the gyrokinetic Poisson equation [3]

$$\rho_s^2 \nabla_\perp \cdot n \nabla_\perp \frac{e\phi}{T_e} = -\delta n, \tag{6}$$

where $\rho_s^2 = \rho_i^2 T_e/T_i$ is the ion gyroradius in terms of the electron temperature. Eqs. (5) and (6) give the magnitude of the ambipolar potential and field as

$$\frac{e\phi(r)}{T_i} = -\int_0^r dr' \frac{1}{2nr'} \int_0^{r'} sds[n''(s) + n'(s)/s], \tag{7}$$

$$E(r) = \frac{T_i}{2nre} \int_0^r sds[n''(s) + n'(s)/s]. \tag{8}$$

Using $w << r_0$ we find that the maximum magnitude of the electric field occurs at $r \simeq r_0 + w^2/(2r_0)$. This equation, originating from the extra charge density term given by Eq. 5, has the form of force balance,

$$enE_\perp = (1/2)(T_e/T_i)\nabla_\perp p_i. \tag{9}$$

This effect is present with any equilibrium density gradient, but can be more pronounced near the boundary layer in a H-mode tokamak discharge, and produce a significant radial electric field well, contributing to long radial wavelength zonal flow. Steep density profiles have been observed on many tokamaks, with some measurements of associated radial electric field wells. See Theiler et al[4] for results on Alcator C-Mod, Diallo et al[7] for results on NSTX, Cordey et al[5] and Hillesheim et al[6] for results on JET, Burrell et al[8] for DIII-D, and Hubbard et al[9] for JT-60U.

Using data from these sources and fitting the observed pedestal with the form given by Eq. 3, we examine the form and magnitude of this field for some observed equilibrium

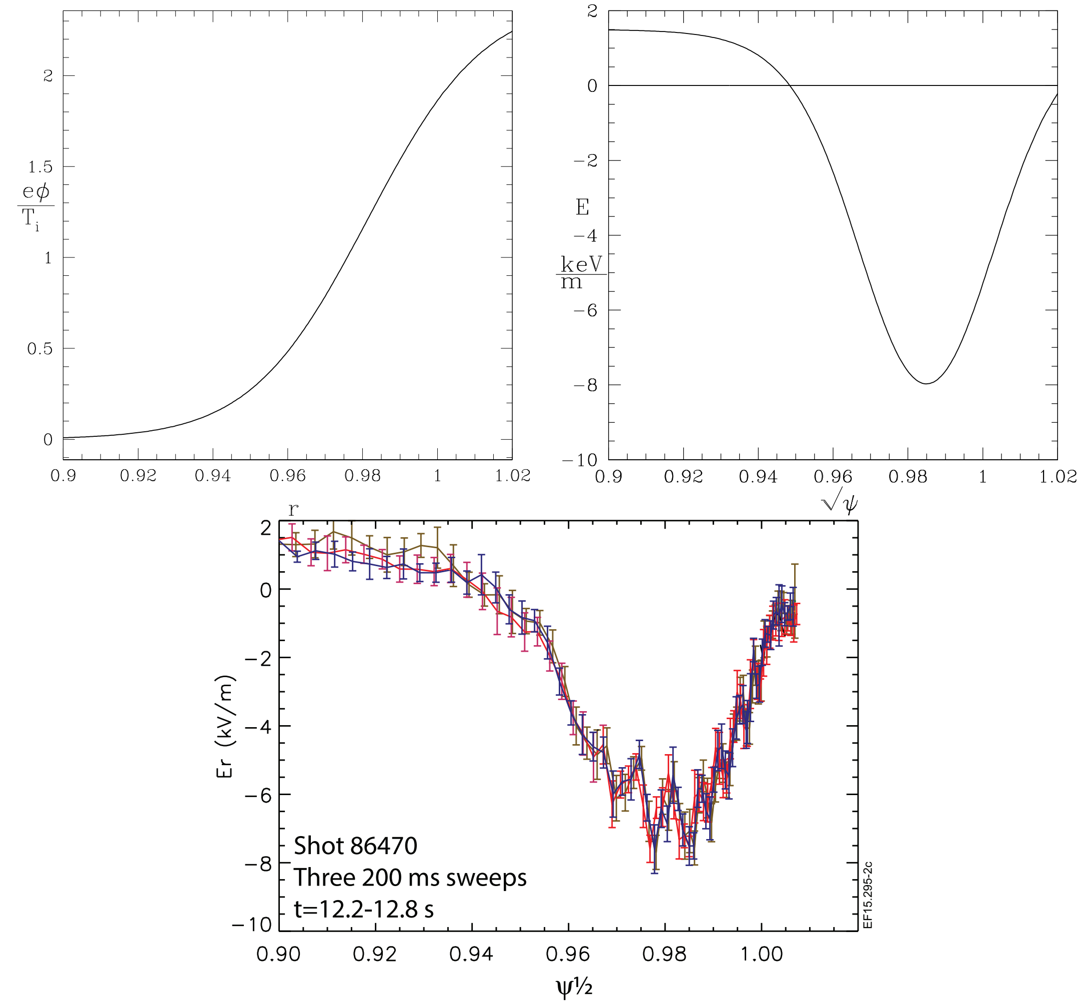

FIG. 2: Electric potential and electric field caused by the charge density resulting from ion cylotron motion in the density distribution given by Eq. 3, and the electric field measuremtnt from JET Ohmic discharge, shot 86470.

configurations. Results from JET H-mode discharges are difficult to use because of the presence of radial fields associated with plasma rotation. However, good data exists for an Ohmic discharge, shot 86470, with parameters (using normalized $\sqrt{\psi}$ as radius) $a = 102$, and $r_0 = 97$, $w = 2.$, $n_s = .05$, $T_i = 300ev$, giving the plot shown in Fig. 2, including also Fig. 2 of reference [6], reprinted with permission of the authors. The value of E has been moved upward 2 keV/m to match the value in the core. The large electric potential shown in Fig. 2 can be understood from the theoretical predictions given in [3].

Shown in Fig. 3 is the resulting electric field for NSTX using data from the plots of Figs. 2 and 8 of Diallo et al [7], giving approximately $a = 67cm$, $r_0 = 60.4cm$, $w = 1.2cm$, and

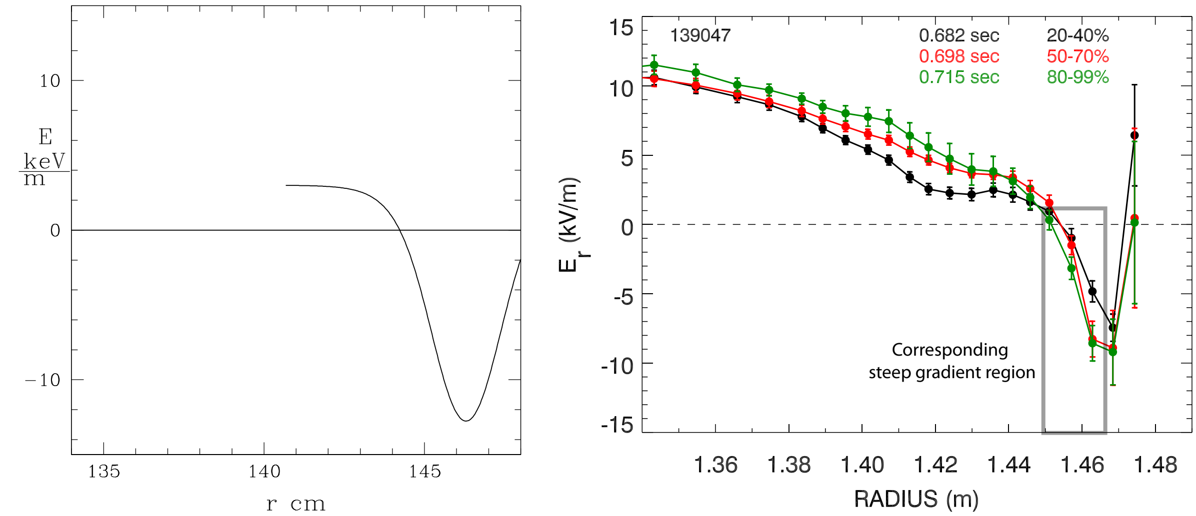

FIG. 3: Electric field caused by the charge density resulting from ion cylotron motion in the density distribution given by Eq. 3, for a NSTX discharge, and the radial electric field observed.

$n_s = .05$, $T_i = 300ev$. The field has been displaced upward by 3 keV/m to better match the value to the left of the pedestal, at about 142 cm, associated with a core plasma rotation. Also shown is Fig. 8 of Diallo et al, reprinted with permission of the authors.

Using data from Theiler et al[4] to estimate Alcator H-mode parameters as $a = 22cm$, $r_0 = 21.3cm$, $n_s = .02$, $T_i = 350eV$, and a pedestal width of $0.3cm$, in Fig. 4 is shown a plot of the electric field obtained from Eq. 7. The field reaches a magnitude of -70 keV/m, much larger than in other devices because of the small pedestal width. The field has been increased by 15 keV/m to better match the value to the left of the pedestal. Also shown is Fig. 3 of Theiler et al, reprinted with permission of the authors.

Published results for DIII-D and JT-60 contain information concerning the density pedestal, but do not include observation of the radial electric field. We have calculated the field using the form of the pedestal, but have no data with which to compare our results.

Of course the exact shape and magnitude of the potential and field depend on the form of the pedestal, and without a numerical fit to this, rather than a simple use of Eq. 3, a detailed comparison cannot be made. In particular, in using this equation we are taking account only of the density gradient, rather than the full pressure gradient as required in Eq. 5. Thus these results must be regarded as very approximate. However, the general shape and magnitude of the results makes gyrokinetic charge density in the presence of a strong

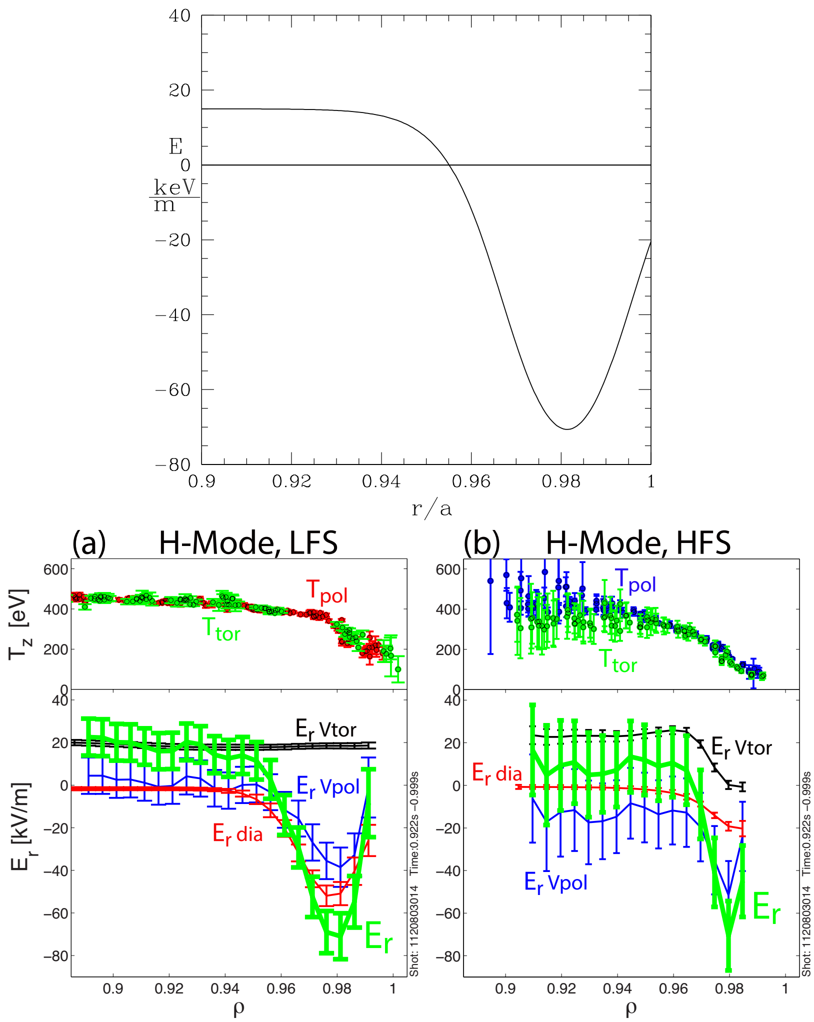

FIG. 4: Electric field caused by the charge density resulting from ion cylotron motion in the density distribution given by Eq. 3, for a Alcator C-Mod H-mode discharge, and the observed temperature profile and radial electric field observed.

inhomogeneity a candidate for the explanation of the observed radial electric field well.

The present paper gives a possible theoretical explanation for the formation of observed radial electric field wells at edge pedestals through finite Larmor radius (FLR) effects of the plasma particles. The well can be regarded as producing a long radial wavelength global zonal flow. The surprising agreement between our model, based on equilibrium profiles with no turbulence, and the experimental measurements based on steady state profiles with turbulence, should be a topic of interest in the tokamak community. It is possible these two totally different states are thermodynamically related. However, initial value electrostatic simulations with turbulence show a rapid modification of this potential [10]. In the future, we may need to carry out simulations based on the fully electromagnetic models as given by, for example, Ref. [11, 12], by connecting microturbulence with MHD equilibrium.

Additionally, we would like to point out that the present calculations regarding the formation of a radial electric field is unrelated to the concept of pressure balance from the gyrokinetic point of view. For example, the ion current associated with our present model, as shown in Fig. 1, based on the calculation of

$$\frac{\mathbf{J}_\perp(\mathbf{x})}{enc_s} = \frac{1}{n}\int \frac{\mathbf{v}_\perp}{c_s} F(\mathbf{x},\mathbf{v}) d\mathbf{v} \tag{10}$$

expressed in terms poloidal velocity is given in black in Fig. 5. By transforming $F(\mathbf{x},\mathbf{v})$ to $F(\mathbf{R},\mathbf{v})$ and performing gyrophase averaging, where $\mathbf{x} = \mathbf{R} + \vec{\rho}$ and $\vec{\rho}$ is the particle gyroradius, the associated ion current based on the gyrokinetic pressure balance of [11]

$$\frac{\mathbf{J}_\perp(\mathbf{x})}{enc_s} \approx \mathbf{b} \times \frac{\rho_s \nabla p_\perp}{nT_e} \tag{11}$$

is given in red in Fig. 5 and $p_\perp = nT$ for the ions and $\mathbf{b} \equiv \mathbf{B}/B$. The result of Eq. (10) is shifted by one cycltron orbit width compared to that from Eq. (11). The difference between the two is due to the fact that the current associated with the present pressure balance is calculated from the lowest order approximation in $k_\perp \rho_i$. Apparently, higher order terms in gyrokinetic theory are needed in order to match the two calculations. The most important message here is that the poloidal velocities v_θ's given in Fig. 5 should not be confused with the poloidal velocities produced by the E_r field at the tokamak edge, which comes from the charge imbalance, δn, in Eq. (5). The δv_θ term associated with the E_r field mentioned in Ref. [12] is finite, but small, compared to the present calculation based on Eq. (11).

In closing, let us consider an additional effect of this gyrokinetic charge density. The corresponding $E \times B$ velocity for the particles in the radial potential becomes

$$\frac{< v_{E\times B} >}{c_s} = \rho_s \left(\frac{\partial}{\partial r}\frac{e\phi}{T_e}\right)\mathbf{e}_\theta = -\frac{\rho_s T_i}{rT_e}\int_0^r sds \frac{n''(s) + n'(s)/s}{2n(s)}\mathbf{e}_\theta, \tag{12}$$

where c_s is the ion acoustic speed.

The induced current is then

$$\frac{J_\theta}{en_0 c_s} = -\sqrt{\frac{T_i}{T_e}}\frac{\rho_i}{r}\frac{n}{n_0}\int_0^r rdr\frac{(n'' + n'/r)}{2n} = \sqrt{\frac{T_i}{T_e}}F(\rho_i, w) \tag{13}$$

with

$$F(\rho_i, w) = -\frac{n\rho_i}{n_0 r}\int_0^r rdr\frac{(n'' + n'/r)}{2n}. \tag{14}$$

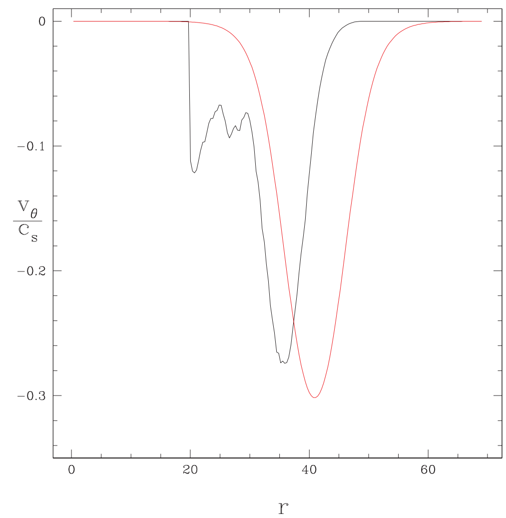

FIG. 5: Comparisons between the direct calculation of v_θ from the actual particles and that from the pressure balance.

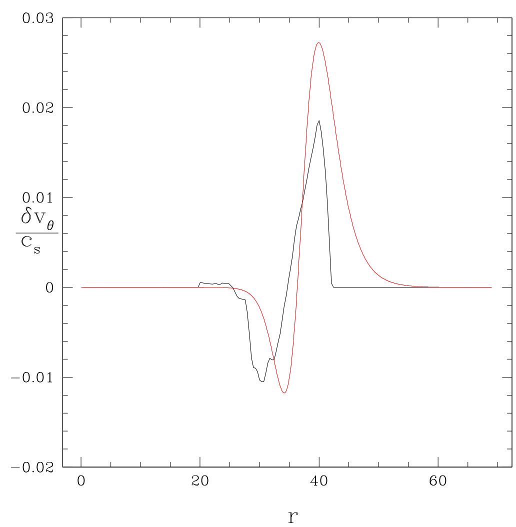

FIG. 6: Difference in poloidal velocity for particles and gyro centers moving in the potential given in Eq. 7 as a function of minor radius, in cm, for the model test case of Fig. 1.

Furthermore, because of the FLR of the ions, the $E \times B$ velocity due to this potential is different for the electrons and the ions, there is a net current associated with this velocity. Consequently, the perpendicular current due to the equilibrium pressure gradient [11] is now modified by a higher order term as predicted by Lee [12], which may become significant in regions with sharp pressure gradient in tokamaks. Namely, Eq. (11) now becomes [12]

$$\frac{\mathbf{J}_\perp(\mathbf{x})}{enc_s} \approx \mathbf{b} \times \frac{\rho_s \nabla p_\perp}{nT_e}\left(1 - \frac{1}{4}\rho_i^2 \frac{\nabla_\perp^2 p_\perp}{p_\perp}\right). \tag{15}$$

We thus examine the difference in particle and guiding center poloidal velocity in the presence of this potential. In Fig. 6 is shown a simulation of this difference. The radial potential given by Eq. 7 was used with the parameters of our test case, and a particle distribution given by Eq. 3 was advanced in time, with the particle and guiding center poloidal velocities recorded in radial bins every time step. The potential causes a difference in poloidal velocity of particles and guiding centers, and hence also between particles and electrons. An approximation for this function, $\rho_i^3 n' \nabla^2 n/(2n)$ used in [12], is shown in red. Interestingly, Eq. (15) is related to the Woltjer-Taylor state [13] of $\nabla \times \mathbf{B} = \alpha \mathbf{B}$, via Ampere's law, as

$$\nabla p_\perp \left(1 - \frac{1}{4}\rho_i^2 \frac{\nabla_\perp^2 p_\perp}{p_\perp}\right) = 0, \tag{16}$$

which can be obtained by multiplying Eq. (15) by $\times\mathbf{b}$. It then gives the solutions of

$$\nabla p_\perp = 0,$$

and, at large radius,

$$p_\perp = exp(-2r/\rho_i).$$

These expressions are, therefore, closely related to the hyperbolic tangent profile used in the present study. Thus, the system under our consideration is indeed a minimum energy state associated with Woltjer-Taylor.

Finally, we should mention that a similar attempt was made earlier by Hazeltine et al. [14] to explain the H-mode edge based on the charge separation due to the FLR effects [1]. However, without using the quasneurality condition, i.e., the gyrokinetic Poisson's equation, Eq. (6), as we have done here, their calculations were incorrect.

* This work was partially supported by the U.S. Department of Energy Grants DE-AC02-09CH11466. We would like to thank Ron Bell, Alain Brizard, Tim Stoltzfus-Dueck and Weixing Wang for useful discussions.

---

[1] W. W. Lee, "Gyrokinetic Approach in Particle Simulation," Phys. Fluids **26**, 556 (1983).

[2] R. B. White, *The Theory of Toroidally Confined Plasmas, third edition*, Imperial College Press, p330 (2014)

[3] W. W. Lee and R.A. Kolesnikov, Phys. Plasmas, **16**, 044506 (2009).

[4] C. Theiler, R.M. Churchill, B. Lipschultz, M. Landreman, D.R. Ernst, J.W. Hughes, P.J. Catto, R.I. Parra, I.H. Hutchinson, M.L. Reinke, A.E. Hubbard, E.S. Marmar, J.T. Terry, J.R. Walk, and the Alcator C-Mod team, Nucl. Fusion **54**, 083017 (2014).

[5] J.G. Cordey, B. Balet, D.V. Bartlett, R. V. Budney, J.P. Christiansen, G.D. Conway, L.G. Erikson, G. M. Fishpool, C. W. Gowers, J.C.M. de Haas, P.J. Harbour, L.D. Horton, A.C. Howman, J. Jacquinot, W. Kerner, C.G. Lowry, R.D. Monk, P. Nielsen, E. Righi, F.G. Rimini, G. Saibene, R. Sartori, B. Schunk, A.C.C. Sips, R.J. Smith, M.F. Stamp, D.F.H. Start, K. Thomsen, B.J.D. Tubbing, M.G. von Hellerman, Nucl Fus, **39**, 301 (1999).

[6] J.C. Hillesheim, E. Delabie, H. Meyer, C. F. Maggi, L. Meneses, E. Poli, and JET Contributors, Phys. Rev. Letters, **116**, 065002 (2016).

[7] A. Diallo, J. Canik, T. Goerler, S.H. Ku, G.J. Kramer, T. Osborne, P. Snyder, D.R. Smith, W. Guttenfelder, R.E. Bell, D.P. Boyle, C.S. Chang, B.P. LeBlanc, R. Maingi, M. Podesta, and S. Sabbagh, Nucl Fus, **53**, 1 (2013).

[8] K.H. Burrell, T.N. Carlstrom, E.J. Doyle, D. Finkenthal, P. Gohil, R.J. Grobner, D.L. Hillis, J. Kim, H. Matsumoto, R.A. Moyer, T.H. Osborne, C.L. Rettig, W.A. Peebles, T.L. Rhodes, H. StJohn, R.D. Stambaugh, M.R. Wade, and J.G. Watkins, Plasma Phys and Controlled Nucl Fus, **34**, 1859 (1992).

[9] A.E. Hubbard, Plasma Phys and Controlled Nucl Fus, **42**, A15 (2000).

[10] W. X. Wang, private communication, 2016.

[11] W. W. Lee and H. Qin, Phys. Plasmas **10**, 3196 (2003).

[12] W. W. Lee, Phys. Plasmas **23**, 070705 (2016).

[13] J. B. Taylor, Phys. Rev. Lett. **33**, 1139 (1974).

[14] R. D. Hazeltine, H. Xiao, and P. M. Valanju, Phys. Fluids B **5**, 4011 (1993).

Princeton Plasma Physics Laboratory
Office of Reports and Publications

Managed by
Princeton University

under contract with the
U.S. Department of Energy
(DE-AC02-09CH11466)

P.O. Box 451, Princeton, NJ 08543
Phone: 609-243-2245
Fax: 609-243-2751

E-mail: publications@pppl.gov

Website: http://www.pppl.gov